Physics Letters B 805 (2020) 135428

Contents lists available at ScienceDirect

Physics Letters B

www.elsevier.com/locate/physletb

Measurement of the ^{3}He spin-structure functions and of neutron (^{3}He) spin-dependent sum rules at $0.035 \leq Q^2 \leq 0.24$ GeV^2

Jefferson Lab E97-110 Collaboration

V. Sulkosky [a,b,c], J.T. Singh [c], C. Peng [d], J.-P. Chen [b], A. Deur [c,b,*], S. Abrahamyan [e], K.A. Aniol [f], D.S. Armstrong [a], T. Averett [a], S.L. Bailey [a], A. Beck [g], P. Bertin [h], F. Butaru [i], W. Boeglin [j], A. Camsonne [h], G.D. Cates [c], C.C. Chang [k], Seonho Choi [i], E. Chudakov [b], L. Coman [j], J.C. Cornejo [f], B. Craver [c], F. Cusanno [l], R. De Leo [m], C.W. de Jager [b,1], J.D. Denton [n], S. Dhamija [o], R. Feuerbach [b], J.M. Finn [a], S. Frullani [p,q], K. Fuoti [a], H. Gao [d], F. Garibaldi [p,q], O. Gayou [g], R. Gilman [b,r], A. Glamazdin [s], C. Glashausser [r], J. Gomez [b], J.-O. Hansen [b], D. Hayes [t], B. Hersman [u], D.W. Higinbotham [b], T. Holmstrom [a,n], T.B. Humensky [c], C.E. Hyde [t], H. Ibrahim [t,v], M. Iodice [l], X. Jiang [r], L.J. Kaufman [w], A. Kelleher [a], K.E. Keister [a], W. Kim [x], A. Kolarkar [o], N. Kolb [o], W. Korsch [o], K. Kramer [a,d], G. Kumbartzki [r], L. Lagamba [m], V. Lainé [b,h], G. Laveissiere [h], J.J. Lerose [b], D. Lhuillier [y], R. Lindgren [c], N. Liyanage [c,b], H.-J. Lu [z], B. Ma [g], D.J. Margaziotis [f], P. Markowitz [j], K. McCormick [r], M. Meziane [d], Z.-E. Meziani [i], R. Michaels [b], B. Moffit [a], P. Monaghan [g], S. Nanda [b], J. Niedziela [w], M. Niskin [j], R. Pandolfi [aa], K.D. Paschke [w], M. Potokar [ab], A.J.R. Puckett [c], V.A. Punjabi [ac], Y. Qiang [g], R. Ransome [r], B. Reitz [b], R. Roché [ad], A. Saha [b], A. Shabetai [r], S. Širca [ab], K. Slifer [i], R. Snyder [c], P. Solvignon [i], R. Stringer [d], R. Subedi [ae], W.A. Tobias [c], N. Ton [c], P.E. Ulmer [t], G.M. Urciuoli [l], A. Vacheret [y], E. Voutier [af], K. Wang [c], L. Wan [g], B. Wojtsekhowski [b], S. Woo [x], H. Yao [i], J. Yuan [r], X. Zhan [g], X. Zheng [ag], L. Zhu [g]

[a] College of William and Mary, Williamsburg, VA 23187-8795, USA
[b] Thomas Jefferson National Accelerator Facility, Newport News, VA 23606, USA
[c] University of Virginia, Charlottesville, VA 22904, USA
[d] Duke University, Durham, NC 27708, USA
[e] Yerevan Physics Institute, Yerevan 375036, Armenia
[f] California State University, Los Angeles, Los Angeles, CA 90032, USA
[g] Massachusetts Institute of Technology, Cambridge, MA 02139, USA
[h] LPC Clermont-Ferrand, Université Blaise Pascal, CNRS/IN2P3, F-63177 Aubière, France
[i] Temple University, Philadelphia, PA 19122, USA
[j] Florida International University, Miami, FL 33199, USA
[k] University of Maryland, College Park, MD 20742, USA
[l] Istituto Nazionale di Fisica Nucleare, Sezione di Roma, Piazzale A. Moro 2, I-00185 Rome, Italy
[m] Istituto Nazionale di Fisica Nucleare, Sezione di Bari and University of Bari, I-70126 Bari, Italy
[n] Longwood University, Farmville, VA 23909, USA
[o] University of Kentucky, Lexington, KY 40506, USA
[p] Istituto Nazionale di Fisica Nucleare, Sezione di Roma, I-00185 Rome, Italy
[q] Istituto Superiore di Sanità, I-00161 Rome, Italy
[r] Rutgers, The State University of New Jersey, Piscataway, NJ 08855, USA
[s] Kharkov Institute of Physics and Technology, Kharkov 310108, Ukraine
[t] Old Dominion University, Norfolk, VA 23529, USA
[u] University of New Hampshire, Durham, NH 03824, USA
[v] Cairo University, Cairo, Giza 12613, Egypt
[w] University of Massachusetts-Amherst, Amherst, MA 01003, USA
[x] Kyungpook National University, Taegu City, South Korea

* Corresponding author at: Thomas Jefferson National Accelerator Facility, Newport News, VA 23606, USA.
E-mail address: deurpam@jlab.org (A. Deur).
[1] Deceased.

https://doi.org/10.1016/j.physletb.2020.135428

[y] DAPNIA/SPhN, CEA Saclay, F-91191 Gif-sur-Yvette, France
[z] Department of Modern Physics, University of Science and Technology of China, Hefei 230026, China
[aa] Randolph-Macon College, Ashland, VA 23005, USA
[ab] Institut Jozef Stefan, University of Ljubljana, Ljubljana, Slovenia
[ac] Norfolk State University, Norfolk, VA 23504, USA
[ad] Florida State University, Tallahassee, FL 32306, USA
[ae] Kent State University, Kent, OH 44242, USA
[af] LPSC, Université Joseph Fourier, CNRS/IN2P3, INPG, F-38026 Grenoble, France
[ag] Argonne National Laboratory, Argonne, IL 60439, USA

ARTICLE INFO

Article history:
Received 5 March 2020
Received in revised form 9 April 2020
Accepted 10 April 2020
Available online 23 April 2020
Editor: D.F. Geesaman

ABSTRACT

The spin-structure functions g_1 and g_2, and the spin-dependent partial cross-section σ_{TT} have been extracted from the polarized cross-sections differences, $\Delta\sigma_{\parallel}(\nu, Q^2)$ and $\Delta\sigma_{\perp}(\nu, Q^2)$ measured for the $^3\vec{\mathrm{He}}(\vec{e}, e')X$ reaction, in the E97-110 experiment at Jefferson Lab. Polarized electrons with energies from 1.147 to 4.404 GeV were scattered at angles of 6° and 9° from a longitudinally or transversely polarized ^{3}He target. The data cover the kinematic regions of the quasi-elastic, resonance production and beyond. From the extracted spin-structure functions, the first moments $\overline{\Gamma_1}(Q^2)$, $\Gamma_2(Q^2)$ and $I_{TT}(Q^2)$ are evaluated with high precision for the neutron in the Q^2 range from 0.035 to 0.24 GeV^2. The comparison of the data and the chiral effective field theory predictions reveals the importance of proper treatment of the Δ degree of freedom for spin observables.

The study of nucleon spin structure has been actively pursued over the past thirty years [1], both theoretically and experimentally at several laboratories, including CERN [2], SLAC [3,4], DESY [5,6] and Jefferson Lab (JLab) [7–15] using doubly polarized inclusive lepton scattering. This research provides a powerful means to study the strong force and its gauge theory, quantum chromodynamics (QCD). They are well tested at high momenta where perturbative expansions in α_s, QCD's coupling, are feasible. Extensive data also exist at intermediate momenta. Yet, at the low momenta characterizing the domain of quark confinement, there are no precision data. There, studies are complicated by 1) the difficulty of finding calculable observables, and 2) the inapplicability of perturbative QCD due to the steep increase of α_s [16]. Sum rules offer a remarkable opportunity to address the first problem by equating measurable moments of structure functions to calculable Compton scattering amplitudes. The second challenge demands the use of non-perturbative techniques such as lattice QCD, or of effective approaches such as chiral effective field theory (χEFT) [17]. In χEFT, the effective hadronic degrees of freedom, relevant at low momenta, are used –rather than the fundamental ones (partons) explicit only at large momenta– and the χEFT Lagrangian structure is established by the symmetries of QCD.

A spin-dependent sum rule of great interest is the one of Gerasimov, Drell, and Hearn (GDH) [18]. It links an integral over the excitation spectrum of the helicity-dependent photoabsorption cross-sections to the target's anomalous magnetic moment κ. The sum rule stems from causality, unitarity, and Lorentz and gauge invariances. Its expression for a spin-½ target is:

$$\int_{\nu_0}^{\infty} \left[\sigma_{1/2}(\nu) - \sigma_{3/2}(\nu)\right] \frac{d\nu}{\nu} = -\frac{2\pi^2\alpha}{M_t^2}\kappa^2, \tag{1}$$

where M_t is the target mass, ν the photon energy, ν_0 the inelastic threshold and α is the fine-structure constant. The ½ (3/2) indicates that the photon helicity is parallel (anti-parallel) to the target spin. The GDH sum rule can be applied to various polarized targets such as ^{3}He and the neutron, with predictions of −498.0 and −232.5 μb, respectively. The sum rule was verified on the proton by the MAMI, ELSA, and LEGS experiments [19] with circularly polarized photons of up to $\nu \approx 3$ GeV.

Starting in the 1980's, generalizations of the integrand for virtual photon absorption were proposed [20–22], e.g.:

$$I_{TT}(Q^2) \equiv \frac{M_t^2}{8\pi^2\alpha}\int_{\nu_0}^{\infty} \frac{\kappa_f(\nu, Q^2)}{\nu}\frac{\sigma_{1/2}(\nu, Q^2) - \sigma_{3/2}(\nu, Q^2)}{\nu} d\nu$$
$$= \frac{2M_t^2}{Q^2}\int_0^{x_0}\left[g_1(x, Q^2) - \frac{4M_t^2}{Q^2}x^2 g_2(x, Q^2)\right]dx, \tag{2}$$

where ν is the energy transfer, Q^2 the four-momentum transfer squared, $x = Q^2/2M_t\nu$ is the Bjorken scaling variable, $x_0 = Q^2/2M_t\nu_0$, and g_1 and g_2 are the spin structure functions. κ_f, the virtual photon flux, normalizes the partial cross-sections $\sigma_{1/2,3/2}$ [1]. Its form is conventional and we will use here the Hand convention [23], $\kappa_f = \nu - Q^2/2M$. Different choices of convention have lead to different generalization of the GDH sum [22]. However, the value of $I_{TT}(Q^2)$ is independent of the choice of κ_f since it also normalizes the $\sigma_{1/2,3/2}$, as shown explicitly when $I_{TT}(Q^2)$ is expressed with g_1 and g_2. These relations extend the integrand to $Q^2 > 0$. The sum rule itself was generalized by Ji and Osborne [24] using a dispersion relation involving the forward virtual Compton scattering amplitude $S_1(\nu, Q^2)$ in the $\nu \to 0$ limit:

$$\overline{\Gamma_1}\left(Q^2\right) \equiv \int_0^{x_0} g_1(x, Q^2)dx = \frac{Q^2}{8}\overline{S_1}(0, Q^2), \tag{3}$$

where the bar indicates exclusion of the elastic contribution. This relation, valid at any Q^2, can be applied back to Eq. (2), equating the moment $I_{TT}(Q^2)$ to $A_{TT}(\nu, Q^2)$, the spin-flip doubly virtual Compton scattering amplitude in the $\nu \to 0$ limit. The amplitudes $\overline{S_1}(0, Q^2)$ and $A_{TT}(0, Q^2)$ are calculable, e.g. in QCD as four-point functions using lattice techniques [25], or by χEFT. Eqs. (2) or (3) can then be used to compare these calculations to experimental data. Such data became available at intermediate [7–12] and large Q^2 [6] in the 1990s and 2000s. Their lowest Q^2 points revealed tensions with the available χEFT calculations of $\overline{S_1}(0, Q^2)$ and $A_{TT}(0, Q^2)$ [26,27]. The discrepancies between data and calculations can be due to the Q^2 coverage of the experiments being

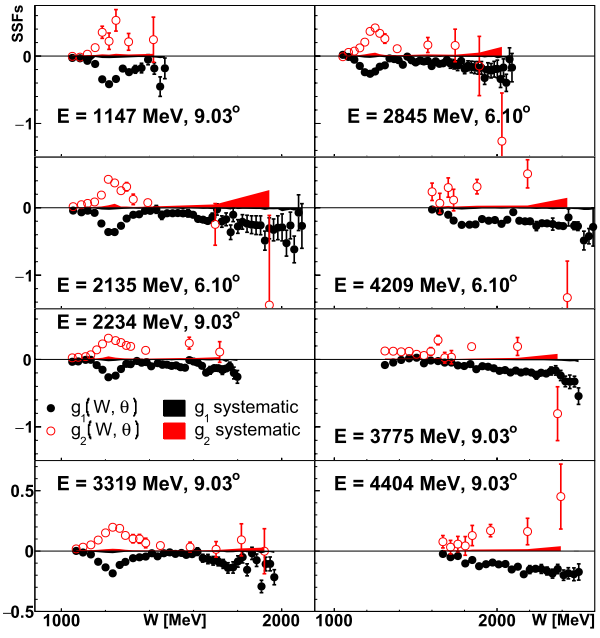

Fig. 1. Spin structure functions (SSFs) $g_1^{^3\mathrm{He}}$ and $g_2^{^3\mathrm{He}}$ at fixed θ and E, versus W. The error bars (bands) provide the statistical (systematic) uncertainty.

not low enough for a valid comparison with χEFT, and/or to the calculations themselves. The data [9–11] showed the importance for χEFT calculations to account for the first excited state (the $\Delta(1232)$) beyond the nucleon ground state. The data also revealed the need for measuring spin moments at Q^2 low enough so that χEFT calculations can be accurately tested.

The other spin structure function g_2 is expected to obey the Burkhardt–Cottingham (BC) sum rule [28]:

$$\Gamma_2(Q^2) \equiv \int_0^1 g_2(x, Q^2)dx = 0\,, \tag{4}$$

a super-convergence relation, i.e. implicitly independent of Q^2, derived from the dispersion relation for the Compton scattering amplitude $S_2\left(Q^2\right)$ [21]. The BC sum rule's validity depends on the convergence of the integral and assumes that g_2 is well-behaved as $x \to 0$ [29].

We present here data on g_1, g_2 and $\sigma_{\mathrm{TT}} \equiv (\sigma_{1/2} - \sigma_{3/2})/2$ on ^{3}He, and of $\overline{\Gamma_1}$, Γ_2 and I_{TT} for the neutron, for $0.035 \leq Q^2 \leq 0.24$ GeV^2 from experiment E97-110 [30,31]. Data were acquired in Hall A [32] at JLab. We measured the inclusive reaction $^3\vec{\mathrm{He}}(\vec{\mathrm{e}}, \mathrm{e}')$ with a longitudinally polarized electron beam scattered from longitudinally or transversely (in-plane) polarized ^{3}He [32]. Eight beam energies E and two scattering angles θ were used to cover kinematics at constant Q^2, see Fig. 1. The data cover invariant mass $W = \sqrt{M^2 + 2M\nu - Q^2}$ (M is the nucleon mass) values from the elastic up to 2.5 GeV; however, only the results above the pion production threshold ($W = 1.073$ GeV) are discussed here. Spin asymmetries and absolute cross-sections were both measured. The beam polarization was flipped pseudo-randomly at 30 Hz and Møller and Compton polarimeters [32] measured it to average at $75.0 \pm 2.3\%$. The beam current ranged from 1 to 10 μA depending on the trigger rate. The data acquisition rate was limited to 4 kHz to keep the deadtime below 20%.

The ^{3}He target was polarized by spin-exchange optical pumping (SEOP) [33]. Two sets of Helmholtz coils providing a parallel or transverse 2.5 mT uniform field allowed us to orient the ^{3}He spins longitudinally or perpendicularly to the beam direction. The target had about 12 atm of ^{3}He gas in a glass cell consisting of two connected chambers. The SEOP process occurred in the upper chamber, which was illuminated with 90 W of laser light at a wavelength of 795 nm. The electron beam passed through a lower chamber made of a 40 cm-long cylinder with a diameter of 2 cm and hemispherical glass windows at both ends. Two independent polarimetries monitored the ^{3}He polarization: nuclear magnetic resonance (NMR) and electron paramagnetic resonance (EPR). The NMR system was calibrated using adiabatic fast passage and the known thermal equilibrium polarization of water. The polarization was independently cross-checked by measuring the elastic ^{3}He asymmetry. The average in-beam target polarization was $(39.0 \pm 1.6)\%$.

The scattered electrons were detected by a High Resolution Spectrometer (HRS) [32] with a lowest scattering angle reachable of 12.5°. A horizontally-bending dipole magnet [34] was placed in front of the HRS so that electrons with scattering angles of 6° or 9° could be detected. The HRS detector package consisted of a pair of drift chambers for tracking, a pair of scintillator planes for triggering and a gas Cherenkov counter, together with a two layer electromagnetic calorimeter for particle identification. Details of the experimental set-up and its performance can be found in [30,31].

The g_1 and g_2 spin structure functions were extracted from the cross-section differences $\Delta\sigma_{\parallel} \equiv \frac{d^2\sigma^{\downarrow\Uparrow}}{d\Omega dE'} - \frac{d^2\sigma^{\uparrow\Uparrow}}{d\Omega dE'}$ and $\Delta\sigma_{\perp} \equiv \frac{d^2\sigma^{\downarrow\Rightarrow}}{d\Omega dE'} - \frac{d^2\sigma^{\uparrow\Rightarrow}}{d\Omega dE'}$ for the case where the target polarization is aligned parallel or perpendicular, respectively, to the beam direction:

$$g_1 = \frac{MQ^2\nu}{4\alpha^2}\frac{E}{E'}\frac{1}{E+E'}\left[\Delta\sigma_{\parallel} + \tan\left(\frac{\theta}{2}\right)\Delta\sigma_{\perp}\right]$$

$$g_2 = \frac{MQ^2\nu}{8\alpha^2 E'(E+E')}\left[-\Delta\sigma_{\parallel} + \frac{E+E'\cos\,\theta}{E'\sin\,\theta}\Delta\sigma_{\perp}\right].$$

The cross-section differences $\Delta\sigma_{\parallel,\perp}$ were formed by combining longitudinal and transverse asymmetries $A_{\parallel}$ and $A_{\perp}$ with the unpolarized absolute cross-section σ_0: $\Delta\sigma_{\parallel,\perp} = 2\sigma_0 A_{\parallel,\perp}$. Unpolarized backgrounds cancel in $\Delta\sigma$ and polarized background are negligible since only ^{3}He nuclei are significantly polarized. The asymmetries were corrected for the beam and target polarizations, as well as beam charge and data acquisition lifetime asymmetries. The dilution of the asymmetry by unpolarized background canceling that same background in σ_0, such correction is unnecessary when forming $\Delta\sigma$.

The absolute cross-section was obtained by correcting for the finite HRS acceptance and detector inefficiencies. The $1/\nu$ weighting of the GDH sum emphasizes low ν contributions. Thus, contamination from elastic and quasi-elastic events appearing beyond the electroproduction threshold due to detector resolution and radiative tails was carefully studied and corrected on both σ_0 and $\Delta\sigma_{\parallel,\perp}$. The high HRS momentum resolution helped to minimize the contamination. For the neutron moments, the quasi-elastic contamination was studied and subtracted by building a model of our data with guidance from state-of-the-art Faddeev calculations [35] and the MAID [36] model. The estimated uncertainty from the subtraction and the effect of varying the lower limit of integration (to account for below-threshold pion production) were included in our systematic uncertainty. Since g_1 and g_2 are defined in the Born approximation, radiative corrections were applied following Ref. [37] for the unpolarized case and using Ref. [38] to include polarized effects. In the unfolding procedure described in [36], cross-section model or data at lower energy are required. To avoid a model-dependent systematic uncertainty, lower energy data gathered for that purpose during the experiment were used in the unfolding procedure.

The results for g_1 and g_2, and for σ_{TT} on ^{3}He are shown in Fig. 1 and Fig. 2, respectively. The data are provided from the pion

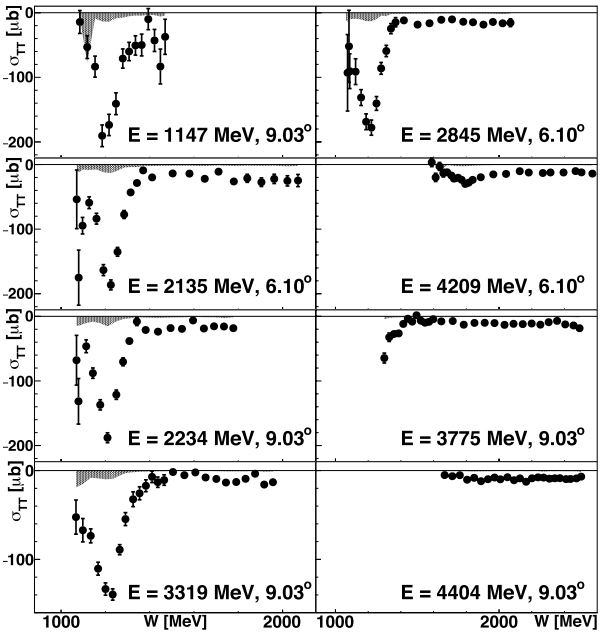

Fig. 2. $\sigma_{TT}^{^3He}$ at fixed θ and E, versus W. The error bars (bands) provide the statistical (systematic) uncertainty.

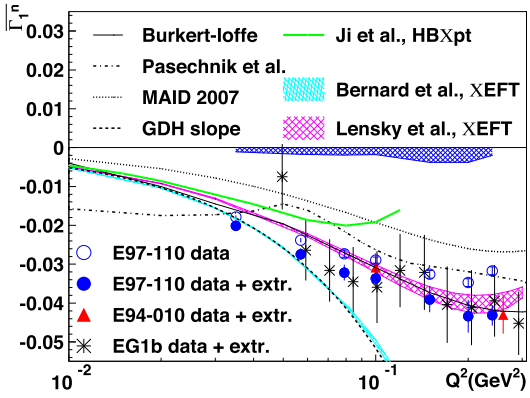

Fig. 3. $\overline{\Gamma_1^n}$ versus Q^2 from this experiment (E97-110), compared to models and earlier JLab data from E94-010 and EG1b. The open circles show the measured partial integral. The filled circles show the full integral with a low-x contribution estimation. The inner error bars on the E97-110 and E94-010 points, often too small to be visible, represent the statistical uncertainties. The combined statistical and uncorrelated systematic uncertainties are shown by the outer error bars. The correlated systematic uncertainty is indicated by the band and typically is about half of the total uncertainty. The GDH sum rule provides $d\overline{\Gamma}_1/dQ^2$ at $Q^2 = 0$ (dashed line), see Eqs. (2) or (3).

threshold. The error bars represent the statistical uncertainty. Systematic uncertainties are shown by the lower band for g_1 and σ_{TT} or the upper band for g_2. The main systematic uncertainties are from the absolute cross-sections (3.5 to 4.5%), beam polarization (3.5%), target polarization (3 to 5%) and radiative corrections (3 to 7%). When combining uncertainties, the uncorrelated ones are added in quadrature. The correlated ones are added linearly. The full systematic uncertainty, shown by the band in Figs. 1 and 2, is the uncorrelated and correlated uncertainties added quadratically. The total systematic for g_1 varies between 12% at low W to 9% at high W, for g_2 it is about 13% over the whole W range, and for σ_{TT} between 11% at low W to 8% at high W.

The data display a prominent feature in the $\Delta(1232)$ region. There, $g_1 \approx -g_2$. This is expected, since the Δ is an $M1$ resonance for which the longitudinal-transverse interference cross-section $\sigma'_{LT} \propto (g_1 + g_2)$ is anticipated to be highly suppressed [22]. Above the Δ, both spin structure functions decrease in magnitude, to increase again as W approaches 2 GeV while still displaying an approximate symmetry indicating the smallness of σ'_{LT}.

To obtain $\overline{\Gamma_1^n}$ and I_{TT}^n, we evaluated g_1, g_2 and σ_{TT} at constant Q^2 by interpolating the fixed θ and E data. The moments were then formed for each value of Q^2 with integration limits from pion threshold to the lowest x value experimentally covered, see tables of the Supplemental Material. The same neutron parameterization as used in Ref. [15] was used to complete the integration down to $x = 0.001$, and the recent Regge parameterization [40] was used for $x < 0.001$. The unmeasured part is about 10% of the full moments. The parameters of the extrapolation models were varied within their estimated ranges, and the variations were combined into the extrapolation uncertainty.

The neutron moments were obtained using the prescription in Ref. [39] which treats the polarized ^{3}He nucleus as an effective polarized neutron. The resulting uncertainty is 6 to 14%, the higher uncertainties corresponding to our lowest Q^2 values. Results for the integrals are given in the tables of the Supplemental Material.

In Fig. 3 our $\overline{\Gamma_1^n}$ is compared to χEFT calculations [27,41,42], models [43,44], the MAID phenomenological parameterization [36] which contains only resonance contributions, and earlier data [7, 10]. Where the Q^2 coverages overlap, our data agree with the earlier data extracted either from the deuteron or ^{3}He. Our precision is much improved compared to the EG1 data [7] and similar to that of the E94-010 [10] data at larger Q^2.

Two χEFT calculations have become available recently [41,42], improving on the earlier ones [26,27]. Those had used different approaches, and different ways to treat for the $\Delta(1232)$ degree of freedom, a critical component of χEFT calculations for baryons. For comparison, we also show in Fig. 3 the older calculation [27] in which the $\Delta(1232)$ is not accounted for. The two state-of-art calculations [41,42] account explicitly for the Δ by computing the $\pi-\Delta$ graphs, but differ in their expansion methods for these corrections and thus on how fast their calculations converge. Comparing them to our data will help to validate the χEFT approach and determine the most efficient calculation technique. Our $\overline{\Gamma_1^n}$ data agree with both calculations up to $Q^2 \approx 0.06$ GeV^2, although a $\sim 1.5\sigma$ offset exists between the calculation [42] and the data. They then agree only with calculation [42], which predicts the plateauing of the data. The deviation for $Q^2 \gtrsim 0.06$ GeV^2 between data and the calculation from Ref. [41] is expected since, as pointed out in [41], a similar deviation is seen with proton data but not for the isovector quantity $\Gamma_1^{(p-n)}$ [12]. The issue thus affects isoscalar combinations and can be traced to the later onset of loop contributions for isoscalar quantities (3 pions, in contrast with 2 pions threshold to isoscalar quantities) [41].

$I_{TT}^n(Q^2)$ is shown in Fig. 4. The integration using only our data, and that with an estimate of the unmeasured low-x part are represented by the open and solid circles, respectively. The open circles should be compared to the MAID result (solid line), which is larger than the data. Our data and the earlier E94-010 data [9] are consistent. As Q^2 decreases, our results drop to around -325 μb, agreeing with the χEFT calculation from Bernard et al. [41] and the earlier one from Ji et al. [27]. The calculation from Lensky et al. [42] displays the same Q^2-dependence as the data but with a systematic shift. Extrapolating the data to $Q^2 = 0$ to check the original GDH sum rule is difficult since the calculations that could be used to guide the extrapolation markedly disagree. Data at lower Q^2 or a theoretical consensus on the Q^2-dependence of I_{TT}^n are needed to address the validity of the original GDH sum rule on the neutron.

$\Gamma_2^n(Q^2)$ is shown in Fig. 5. The stars show the measured integral without low-x extrapolation for the neutron, to be compared with MAID. This model underestimates the higher Q^2 data

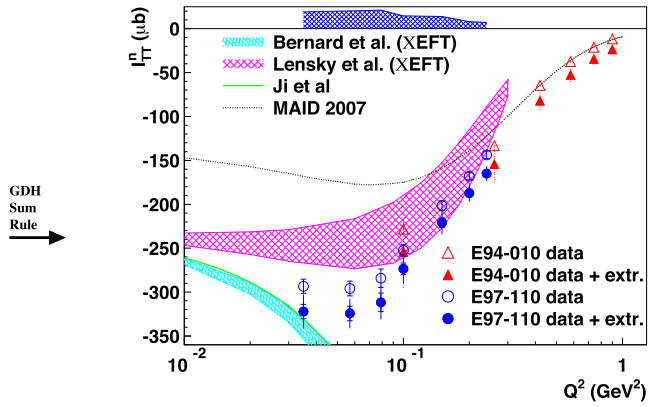

Fig. 4. $I_{TT}^n(Q^2)$ with (filled circles) and without (open circles) the estimated unmeasured low-x contribution. The meaning of the inner and outer error bars and of the band is the same as in Fig. 3. Also shown are χEFT results, MAID (solid line) and earlier E94-010 data [9].

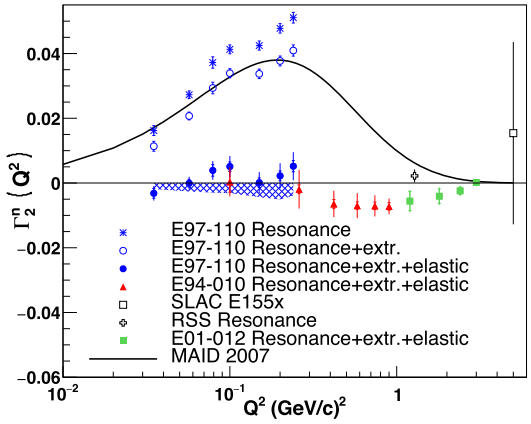

Fig. 5. Γ_2^n versus Q^2. The error band represents the correlated systematic uncertainty from radiative corrections, interpolation of g_2 to constant Q^2, model uncertainties in the neutron extraction from ^{3}He, and the elastic contribution uncertainty. The correlated systematic uncertainty typically represents about half of the total uncertainty. The uncorrelated systematic and statistical uncertainties added in quadrature are shown by the outer error bars. The inner error bars (when visible) represent the statistical uncertainty. Also shown is the MAID model with only resonance contributions.

but agrees well at lower Q^2. The open circles represent the integral including an estimate for the low-x contribution assuming $g_2 = g_2^{WW}$ [4], where g_2^{WW} is the twist-2 part of g_2 [45]. This procedure is used since there are little data to constrain g_2 at low-x. Since it is unknown how well g_2^{WW} matches g_2 there, one cannot reliably assess an uncertainty on the low-x extrapolation and none was assigned. The solid circles show the full integral with the elastic contribution evaluated using Ref. [46]. These data allow us to investigate the BC sum rule in this low-Q^2 region with the caveat of the unknown uncertainty attached to the low-x extrapolation. Under this provision, the data are consistent with the sum rule expectation that $\Gamma_2 = 0$ for all Q^2. They also agree with the earlier results from E94-010 (triangles) [9]. Higher Q^2 data from E01-012 (filled squares) [14], RSS (open crosses) [13], and E155x (open square) [4] are also consistent with zero.

In conclusion, ^{3}He spin structure functions $g_1(\nu, Q^2)$, $g_2(\nu, Q^2)$ and the spin-dependent partial cross-section $\sigma_{TT}(\nu, Q^2)$ were measured at low Q^2. The moments $\overline{\Gamma_1}(Q^2)$, $\Gamma_2(Q^2)$ and $I_{TT}(Q^2)$ of the neutron are extracted at $0.035 \leq Q^2 \leq 0.24$ GeV^2. They are compared to two next-to-leading-order χEFT calculations from two separate groups, Bernard et al. [41] and Lensky et al. calculation [42]. The $\overline{\Gamma_1^n}(Q^2)$ and $I_{TT}^n(Q^2)$ integrals agree with published data at higher Q^2. The data on $\overline{\Gamma_1^n}$ agree reasonably with both recent χEFT calculations. The data on I_{TT}^n disagree with the calculation [42] and that of [41] except at the lowest Q^2 point. That the results for two recent χEFT methods differ, and that they describe with different degrees of success the data underlines the importance of the Δ degree of freedom for spin observables and the sensitivity of χEFT to the consequent π-Δ terms. The earlier E94-010 data had triggered improvement of the χEFT calculations. Now, the precise E97-110 data, taken in the chiral domain, show that yet further sophistication of χEFT is needed before spin observables can be satisfactorily described. Our determination of $\Gamma_2^n(Q^2)$ agrees with the BC sum rule in this low-Q^2 region, with the proviso that g_2^{WW} is used to assess the unmeasured low-x part of Γ_2^n. Analysis of data down to $Q^2 = 0.02$ GeV^2 taken at a different time under different conditions, which requires a different analysis, is currently ongoing. These data and results on σ'_{LT}, the spin polarizabilities γ_0^n and δ_{LT}^n, and moments for ^{3}He will be reported in future publications. All these data, when combined with results [15] obtained on deuteron and future proton data [47] taken at low Q^2, will yield further extensive tests of calculations from χEFT, the leading effective theory of strong interactions at low Q^2, and eventually to QCD once the lattice QCD calculations of the Compton amplitudes involved in the sum rules becomes available.

Declaration of competing interest

The authors declare that they have no known competing financial interests or personal relationships that could have appeared to influence the work reported in this paper.

Acknowledgements

We acknowledge the outstanding support of the Jefferson Lab Hall A technical staff and the Physics and Accelerator Divisions that made this work possible. We thank A. Deltuva, J. Golak, F. Hagelstein, H. Krebs, V. Lensky, U.-G. Meißner, V. Pascalutsa, G. Salmè, S. Scopetta and M. Vanderhaeghen for useful discussions and for sharing their calculations. This material is based upon work supported by the U.S. Department of Energy, Office of Science, Office of Nuclear Physics under contract DE-AC05-06OR23177, and by the NSF under grant PHY-0099557.

Appendix A. Supplementary material

Supplementary material related to this article can be found online at https://doi.org/10.1016/j.physletb.2020.135428.

References

[1] J.P. Chen, A. Deur, Z.E. Meziani, Mod. Phys. Lett. A 20 (2005) 2745;
J.P. Chen, Int. J. Mod. Phys. E 19 (2010) 1893;
S.E. Kuhn, J.-P. Chen, E. Leader, Prog. Part. Nucl. Phys. 63 (2009) 1;
A. Deur, S.J. Brodsky, G.F. De Téramond, Rep. Prog. Phys. 82 (2019) 7.
[2] J. Ashman, et al., European Muon Collaboration, Phys. Lett. B 206 (1988) 364;
D. Adams, et al., Spin Muon (SMC) Collaboration, Phys. Lett. B 396 (1997) 338; Phys. Rev. D 56 (1997) 5330;
V.Y. Alexakhin, et al., COMPASS Collaboration, Phys. Lett. B 647 (2007) 8.
[3] P.L. Anthony, et al., E142 Collaboration, Phys. Rev. D 54 (1996) 6620;
K. Abe, et al., E143 Collaboration, Phys. Rev. D 58 (1998) 112003;
K. Abe, et al., E154 Collaboration, Phys. Rev. Lett. 79 (1997) 26;
P.L. Anthony, et al., E155 Collaboration, Phys. Lett. B 458 (1999) 529.
[4] P.L. Anthony, et al., E155 Collaboration, Phys. Lett. B 553 (2003) 18.
[5] K. Ackerstaff, et al., HERMES Collaboration, Phys. Lett. B 404 (1997) 383;
A. Airapetian, et al., HERMES Collaboration, Phys. Lett. B 442 (1998) 484; Phys. Rev. D 75 (2007) 012007.
[6] A. Airapetian, et al., HERMES Collaboration, Eur. Phys. J. C 26 (2003) 527.

[7] J. Yun, et al., CLAS Collaboration (EG1a experiment), Phys. Rev. C 67 (2003) 055204;
N. Guler, et al., CLAS Collaboration (EG1b experiment), Phys. Rev. C 92 (2015) 055201;
R. Fersch, et al., CLAS Collaboration (EG1b experiment), Phys. Rev. C 96 (2017) 065208.
[8] K. Slifer, et al., E94010 Collaboration, Phys. Rev. Lett. 101 (2008) 022303;
X. Zheng, et al., Jefferson Lab Hall A Collaboration (E99-117 experiment), Phys. Rev. C 70 (2004) 065207;
K. Kramer, et al., Jefferson Lab Hall A Collaboration (E97-103 experiment), Phys. Rev. Lett. 95 (2005) 142002;
D.S. Parno, et al., Jefferson Lab Hall A Collaboration (E06-014 experiment), Phys. Lett. B 744 (2015) 309.
[9] M. Amarian, et al., E94010 Collaboration, Phys. Rev. Lett. 89 (2002) 242301.
[10] M. Amarian, et al., E94010 Collaboration, Phys. Rev. Lett. 92 (2004) 022301.
[11] M. Amarian, et al., E94010 Collaboration, Phys. Rev. Lett. 93 (2004) 152301.
[12] A. Deur, et al., Phys. Rev. Lett. 93 (2004) 212001; Phys. Rev. D 78 (2008) 032001; Phys. Rev. D 90 (2014) 012009.
[13] K. Slifer, et al., Resonance Spin Structure Collaboration, Phys. Rev. Lett. 105 (2010) 101601.
[14] P. Solvignon, et al., Jefferson Lab Hall A Collaboration (E01-012 experiment), Phys. Rev. C 92 (2015) 015208.
[15] K.P. Adhikari, et al., CLAS Collaboration (EG4 experiment), Phys. Rev. Lett. 120 (2018) 062501.
[16] A. Deur, S.J. Brodsky, G.F. de Teramond, Prog. Part. Nucl. Phys. 90 (2016) 1.
[17] V. Bernard, N. Kaiser, U.G. Meissner, Int. J. Mod. Phys. E 4 (1995) 193.
[18] S.B. Gerasimov, Sov. J. Nucl. Phys. 2 (1966) 430; Yad. Fiz. 2 (1965) 598;
S.D. Drell, A.C. Hearn, Phys. Rev. Lett. 16 (1966) 908.
[19] J. Ahrens, et al., GDH Collaboration (MAMI A2), Phys. Rev. Lett. 87 (2001) 022003;
H. Dutz, et al., ELSA GDH Collaboration, Phys. Rev. Lett. 93 (2004) 032003;
S. Hoblit, et al., LSC Collaboration (LEGS experiment), Phys. Rev. Lett. 102 (2009) 172002.
[20] M. Anselmino, B.L. Ioffe, E. Leader, Sov. J. Nucl. Phys. 49 (1989) 136; Yad. Fiz. 49 (1989) 214.
[21] D. Drechsel, B. Pasquini, M. Vanderhaeghen, Phys. Rep. 378 (2003) 99.
[22] D. Drechsel, S.S. Kamalov, L. Tiator, Phys. Rev. D 63 (2001) 114010.
[23] L.N. Hand, Phys. Rev. 129 (1963) 1834.
[24] X.D. Ji, J. Osborne, J. Phys. G 27 (2001) 127.
[25] A.J. Chambers, et al., Phys. Rev. Lett. 118 (24) (2017) 242001.
[26] V. Bernard, T.R. Hemmert, U.G. Meissner, Phys. Rev. D 67 (2003) 076008.
[27] X.D. Ji, C.W. Kao, J. Osborne, Phys. Lett. B 472 (2000) 1.
[28] H. Burkhardt, W.N. Cottingham, Ann. Phys. 56 (1970) 453.
[29] R.L. Jaffe, X.D. Ji, Phys. Rev. D 43 (1991) 724.
[30] Details of JLab E97-110 and relevant theses can be found at http://hallaweb.jlab.org/experiment/E97-110/.
[31] V. Sulkosky, Ph.D. thesis, College of William & Mary, 2007, Williamsburg, Virginia 23187 USA, http://hallaweb.jlab.org/experiment/E97-110/thesis/PhD_thesis_V_Sulkosky.pdf.
[32] J. Alcorn, et al., Jefferson Lab Hall A Collaboration, Nucl. Instrum. Methods A 522 (2004) 294.
[33] T.R. Gentile, P.J. Nacher, B. Saam, T.G. Walker, Rev. Mod. Phys. 89 (2017) 045004.
[34] F. Garibaldi, et al., Jefferson Lab Hall A Collaboration, Phys. Rev. C 99 (2019) 054309.
[35] J. Golak, et al., Phys. Rev. C 65 (2002) 064004; Phys. Rev. C 72 (2005) 054005;
L.P. Yuan, et al., Phys. Rev. C 66 (2002) 054004;
A. Deltuva, et al., Phys. Rev. C 69 (2004) 034004; Phys. Rev. C 70 (2004) 034004; Phys. Rev. C 71 (2005) 054005.
[36] D. Drechsel, O. Hanstein, S.S. Kamalov, L. Tiator, Nucl. Phys. A 645 (1999) 145.
[37] L.W. Mo, Y.S. Tsai, Rev. Mod. Phys. 41 (1969) 205.
[38] I.V. Akushevich, N.M. Shumeiko, J. Phys. G 20 (1994) 513;
I. Akushevich, A. Ilyichev, N. Shumeiko, A. Soroko, A. Tolkachev, Comput. Phys. Commun. 104 (1997) 201.
[39] C. Ciofi degli Atti, S. Scopetta, Phys. Lett. B 404 (1997) 223.
[40] S.D. Bass, M. Skurzok, P. Moskal, Phys. Rev. C 98 (2018) 025209.
[41] V. Bernard, E. Epelbaum, H. Krebs, U.G. Meissner, Phys. Rev. D 87 (2013) 054032.
[42] V. Lensky, J.M. Alarcón, V. Pascalutsa, Phys. Rev. C 90 (2014) 055202, 2019 update: private communication.
[43] V.D. Burkert, B.L. Ioffe, Phys. Lett. B 296 (1992) 223; J. Exp. Theor. Phys. 78 (1994) 619; Zh. Eksp. Teor. Fiz. 105 (1994) 1153.
[44] R.S. Pasechnik, J. Soffer, O.V. Teryaev, Phys. Rev. D 82 (2010) 076007;
R.S. Pasechnik, D.V. Shirkov, O.V. Teryaev, O.P. Solovtsova, V.L. Khandramai, Phys. Rev. D 81 (2010) 016010.
[45] S. Wandzura, F. Wilczek, Phys. Lett. B 72 (1977) 195.
[46] P. Mergell, U.G. Meissner, D. Drechsel, Nucl. Phys. A 596 (1996) 367.
[47] M. Battaglieri, R. De Vita, A. Deur, M. Ripani, spokespersons for Jefferson Lab Experiment E03-006; A. Camsonne, J.-P. Chen, K. Slifer, spokespersons for Jefferson Lab Experiment E08-027.